

# Geochemistry, Geophysics, Geosystems

### RESEARCH ARTICLE

10.1029/2020GC009152

#### **Key Points:**

- Partial melting of underthrusting lower crust alone does not generate sufficient magma to drive arc flare-ups
- Magmatic thickening rate correlates with underthrusting rate and is affected by the relative timescales of heat transfer and underthrusting
- Crustal underthrusting contributes to arc root growth whose subsequent foundering may regulate the tempo of arc magmatism

#### **Supporting Information:**

- · Data Set S1
- · Data Set S2
- · Supporting Information S1

#### Correspondence to:

J. Yang and W. Cao, jiaming@nevada.unr.edu; wenrongc@unr.edu

# Citation:

Yang, J., Cao, W., Gordon, S. M., & Chu, X. (2020). Does underthrusting crust feed magmatic flare-ups in continental arcs? *Geochemistry, Geophysics, Geosystems, 21*, e2020GC009152, https://doi.org/10.1029/2020GC009152

Received 5 MAY 2020 Accepted 16 OCT 2020

© 2020. American Geophysical Union. All Rights Reserved.

# **Does Underthrusting Crust Feed Magmatic Flare-Ups in Continental Arcs?**

Jiaming Yang<sup>1</sup>, Wenrong Cao<sup>1</sup>, Stacia M. Gordon<sup>1</sup>, and Xu Chu<sup>2</sup>

<sup>1</sup>Department of Geological Sciences and Engineering, University of Nevada, Reno, NV, USA, <sup>2</sup>Department of Earth Sciences, University of Toronto, Toronto, ON, Canada

**Abstract** Episodic magmatic flare-ups are documented in many continental arcs worldwide. Yet, the causes of such episodicity and the sources feeding the flare-ups are not well-understood. In this study, we use a 1-D numerical model and scaling analysis to assess the mass balance and thermodynamic feasibility of generating arc magma as a result of partial melting of underthrusted retro-arc lower crust. Results show the magma volumetric flux or magmatic thickening rate, is directly correlated with the crustal underthrusting rate and the relative timescales of heat transfer and underthrusting. For a continental arc with dimensions similar to the Sierra Nevada arc in California, we show with a constant underthrusting rate of 5 km/Myr, the magmatic thickening rate is 0.1-0.3 km/Myr. This is slightly below the baseline of arc magma thickening rate (~0.3 km/Myr) from the mantle wedge and accounts for 10%-30% of the magmatic thickening rate during a flare-up. The cumulative volume of magma generated from the partial melting of a 20-km-thick underthrusted lower crust is on the order of 10<sup>5</sup> km<sup>3</sup>, about 10%-40% of the estimated magma volume generated during a flare-up. Therefore, we argue partial melting of underthrusted lower crust plays a partial or subsidiary role in driving a magmatic flare-up event. Additional melts from the mantle and/or other crustal sources are needed to achieve the observed magmatic output during flare-ups. The arc root developed by partial melting of the underthrusted crust reduces the time needed to obtain the critical thickness for root foundering, thus influencing the tempo of arc magmatism.

#### 1. Introduction

Continental arc magmatism is an important process for the formation of continental crust and most ore deposits (e.g., Condie, 2013; Rudnick, 1995; Stern, 2002). Continental arcs also play a critical role in Earth's long-term carbon cycle through volcanic and metamorphic degassing and chemical weathering (e.g., Cao et al., 2017; Chu et al., 2019; Lee et al., 2015a; McKenzie, 2017). There is growing field and geochemical evidence suggesting that magmatism is episodic and nonsteady state in continental arcs worldwide (Figure 1; e.g., Ardill et al., 2018; Armstrong & Clark, 1988; DeCelles et al., 2009, 2014; Ducea, 2001; Ducea & Barton, 2007; Gehrels et al., 2009; Haschke et al., 2006; Kirsch et al., 2016; Paterson & Ducea, 2015; X. Zhang et al., 2019; Zhu et al., 2015).

Compilations of U/Pb zircon geochronology from igneous rocks and arc-derived sediments show age peaks and troughs defining magmatic "flare-ups" and "lulls," respectively, on the timescales of tens of millions of years (e.g., Paterson & Ducea, 2015). Typically, these flare-ups or high magma flux events last ~30 Myr and are separated by magmatic lulls spanning 20–50 Myr (e.g., Kirsch et al., 2016). Magma generation rates during the lulls in a continental arc are comparable to the rate of mantle-derived primitive magma generation in island arcs (DeCelles et al., 2009), representing a baseline for the magma contribution from the mantle wedge. The Armstrong unit (AU) is used to quantify the baseline magma generation rate, with 1 AU = 30 km<sup>3</sup>/Myr per kilometer length of arc (DeCelles et al., 2009; Reymer & Schubert, 1984). During a flare-up, the magma generation rate reaches 3–4 AU in the upper-middle crust (DeCelles et al., 2009). The AU can be converted to a volumetric flux (km<sup>3</sup>/km<sup>2</sup>/Myr or km/Myr) if the arc width is known. Given a characteristic arc width of 100 km, the baseline 1 AU is ~0.3 km<sup>3</sup>/km<sup>2</sup>/Myr. For flare-ups in continental magmatic arcs, an estimated volumetric flux of ~1 km<sup>3</sup>/km<sup>2</sup>/Myr (~3–4 AU equivalent) is proposed for the main arc and > 0.6 km<sup>3</sup>/km<sup>2</sup>/Myr (>2 AU equivalent) for a broader region from the forearc to the retro-arc (Ratschbacher et al., 2019). This volumetric flux is also referred to as the magmatic thickening rate (km/Myr), representing

YANG ET AL. 1 of 19

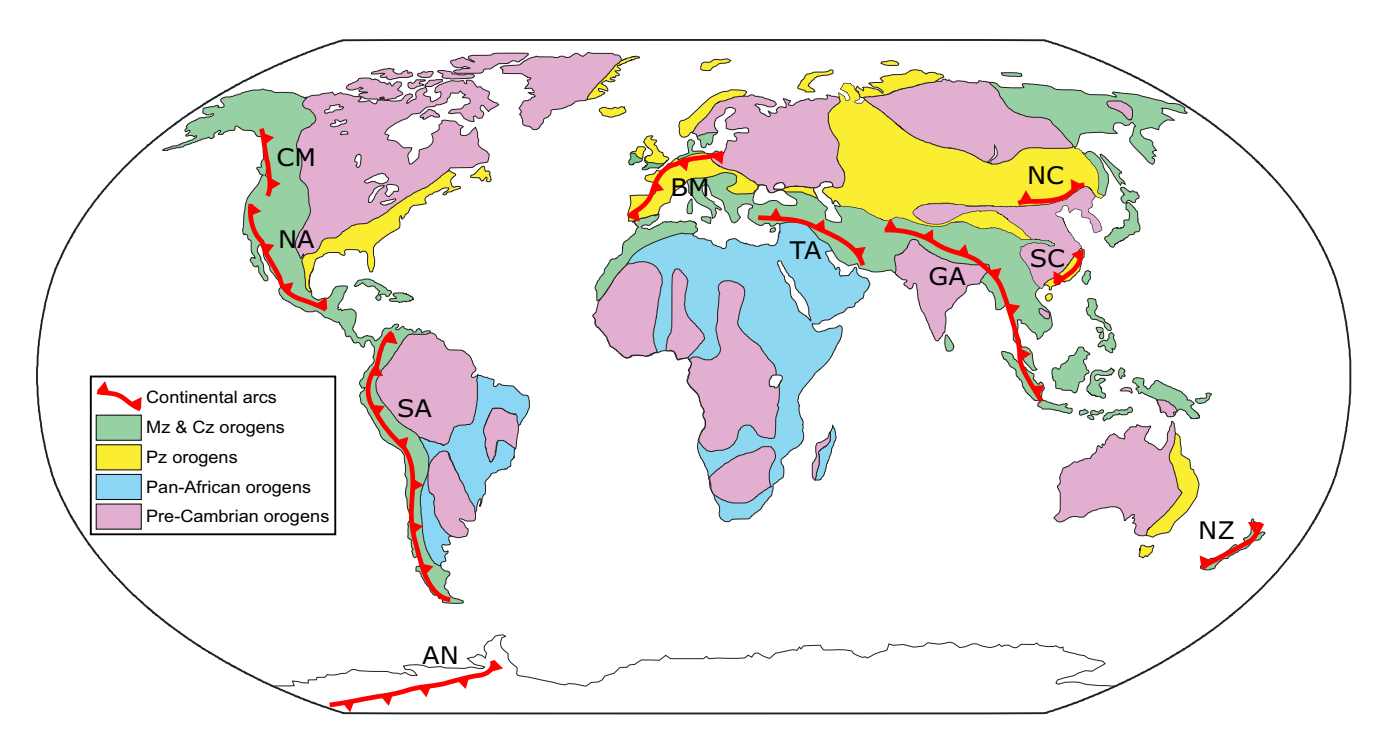


Figure 1. World map in Robinson projection showing the locations of continental arcs where nonsteady state magmatism has been observed. Arc locations are shown as abbreviations: AN = Antarctica (Paulsen et al., 2016), BM = Bohemian Massif (Hajná et al., 2017), CM = Coast Mountains batholith (Cecil et al., 2018), GA = Gangdese-Burma-Sumatra arc (X. Zhang et al., 2019), NC = North China (Cope, 2017), NZ = New Zealand (Schwartz et al., 2017), SA = South American Cordilleran arcs (Kirsch et al., 2016; Pepper et al., 2016), SC = South China (Li et al., 2007), NA = North American Cordilleran arcs (Kirsch et al., 2016; Paterson & Ducea, 2015), TA = Taknar complex (Moghadam et al., 2017). Base map modified from Tsujimori et al. (2006) and Erdman and Lee (2014).

the magmatic contribution to the vertical growth of arc crust (Cao & Paterson, 2016; Jicha & Jagoutz, 2015; Jiang & Lee, 2017; Lee et al., 2015a).

Previous models explaining nonsteady state magmatism focus on: (1) the convergence rate between the subducting and overriding plates regulating magma production (e.g., Pilger, 1984); (2) slab dynamics, including the opening of slab windows and changes in the subduction angle (Z. Zhang et al., 2010); (3) delamination of an eclogitic arc root (e.g., Kay & Kay, 1993; Lee & Anderson, 2015); (4) temporal filtering of mantle-lithosphere interactions where the crust modulates mantle input (De Silva et al., 2015); (5) relamination of material off of the subducting plate and emplacement at the base of the arc crust (e.g., A. D. Chapman et al., 2013; Ducea & Chapman, 2018; Hacker et al., 2011); (6) incorporation of fore-arc sediments into the active arc (Pearson et al., 2017; Sauer et al., 2017, 2018); (7) arc migration into the fertile retro-arc region (J. B. Chapman & Ducea, 2019); and (8) feedback among linked tectonic processes (e.g., DeCelles et al., 2009; Ducea, 2001; Ducea & Barton, 2007).

For North and South America Cordilleran arcs, the temporal correlation between magmatism and plate convergence rate is weak (e.g., Ducea, 2001; Kirsch et al., 2016). Whole rock Nd isotope data show a correlation with magmatism. There is a decrease in  $\varepsilon_{Nd}$  toward more evolved compositions during flare-ups in comparison to increases in  $\varepsilon_{Nd}$  during magmatic lulls (e.g., Ducea, 2001). The negative  $\varepsilon_{Nd}$  excursion is interpreted to signify ~50% contribution from crustal materials to a magmatic flare-up (Ducea, 2001; Ducea & Barton, 2007). Many studies thus hypothesize that magmatism is driven by the repeated incorporation of underthrusted retro-arc crustal materials beneath the arc, boosting melt generation (e.g., DeCelles & Graham, 2015; DeCelles et al., 2009; Ducea, 2001).

However, the thermodynamic feasibility of arc magma generation through partial melting of continental lower crust has not been tested. Quantitative evaluation of such a process requires the inclusion of latent heat associated with melting, the temperature dependency of thermal diffusivity and heat capacity, as well as kinematic conditions such as the underthrusting rate of the retro-arc crust. In this study, we use numerical modeling and scaling analysis to address the following questions: (1) What controls the total volume

YANG ET AL. 2 of 19

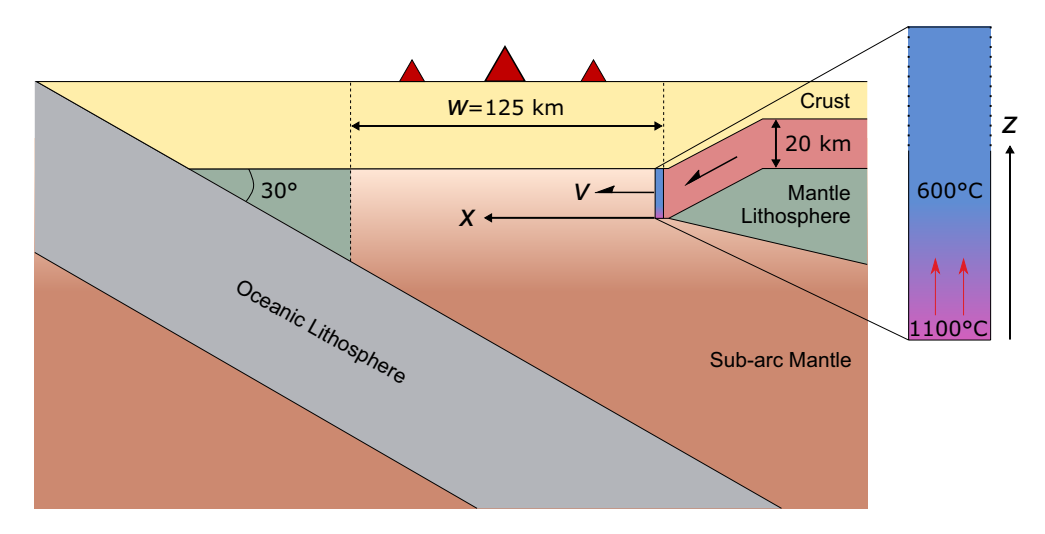


**Figure 2.** Schematic illustration of the numerical model setup, showing model geometry and initial thermal state of the half-space heating model where the underthrusted slab is 600°C everywhere except for the fixed 1100°C bottom boundary.

and rate of magma generation during partial melting of underthrusted crust? (2) Is partial melting of underthrusted crust capable of generating enough arc magma in a relatively short period (~30 Myr) to form a magmatic flare-up? (3) How do the arc root and melts from the mantle interact with the underthrusting crust and contribute to the magmatic flare-up?

# 2. Methods

# 2.1. Initial, Boundary Conditions, and Governing Equation

To investigate arc magma generation during underthrusting, we simulate the 1-D thermal evolution of the underthrusting crust in a numerical model. The vertical temperature profile of the crustal column is coupled with lateral motion, approximating a 2-D cross section of the underthrusting crust. To focus on underthrusting, the model does not include arc root foundering or melting of the mantle. We recognize the importance of these processes and address them in Section 4.

The model consists of a 20-km-thick retro-arc lower crustal slab that is underthrusting into the sub-arc mantle (Figure 2). We use a half-space heating model in which the initial temperature of the underthrusting crustal slab is 600°C everywhere, except for the basal boundary where a constant mantle temperature of 1100°C is enforced. The mantle temperature used in our model is based on the thermal profile of the modern Chilean Andes where the average thermal gradient of the shallow sub-arc mantle below the Moho is  $\sim$ 25°C/km, and the Moho temperature is  $\sim$ 600°C (Syracuse et al., 2010). Implementing this thermal profile into our model, we get 1100°C for the temperature at the base of the underthrusted crust which is 20 km below the 600°C Moho (600°C + 25°C/km × 20 km = 1100°C). For the purpose of investigating first-order thermal effects, we take a simple approach that does not include the geothermal gradient in the underthrusting crust nor cooling of the mantle due to the thickening of the arc crust (Chin et al., 2015). The simulated results thus represent the upper bound of melt generation and the maximum productivity of arc magma. The governing heat equation is as follows:

$$\frac{\partial T}{\partial t} = \frac{\partial}{\partial z} \left[ \kappa \left( T \right) \frac{\partial T}{\partial z} \right] - \frac{L}{C_p(T)} \frac{\partial F}{\partial T} \frac{\partial T}{\partial t} \tag{1}$$

 $\kappa(T)$  is the temperature-dependent diffusivity and  $\frac{L}{C_p} \frac{\partial F}{\partial T} \frac{\partial T}{\partial t}$  is for latent heat (e.g., Bergantz, 1989; Lee et al., 2015b), where L is the total latent heat of fusion absorbed between the solidus and the liquidus of

YANG ET AL. 3 of 19

<sup>a</sup>Lange et al. (1994)

<b>Table 1</b> Parameter Definitions and Values Used in This Study			
Parameter	Symbol	Value	Unit
Thickness of underthrusting crust	z	20	km
Width of the arc	w	125	km
Along strike arc length	l		km
Temperature of crustal slab	$T_{ m crust}$	600	°C
Mantle temperature	$T_{ m mantle}$	1100	°C
Total latent heat of fusion <sup>a</sup>	L	400	${\rm kJ~kg^{-1}}$
Temperature-dependent heat capacity	$C_p(T)$		$\mathrm{Jkg^{-1}K^{-1}}$
Reference thermal diffusivity	κ	$10^{-6}$	$m^2s^{-1}$
Temperature-dependent thermal diffusivity	$\kappa(T)$		$m^2s^{-1}$
Thermal diffusivity (latent heat effect included)	κ'( <i>T</i> )		$m^2s^{-1}$
Equivalent thermal diffusivity (advection included)	$\kappa_{eq}$		$m^2s^{-1}$
Characteristic time of heat transfer	$\tau_{thermal}$		Myr
Melt fraction	F		
Critical melt fraction	$F_{ m crit}$	0.25	
Critical temperature	$T_{ m crit}$		°C
Volume of melt	V		$km^3$
Underthrusting rate	ν		${\rm km}~{\rm Myr}^{-1}$
Underthrusting distance	x		km
Melt area	A		$km^2$
Characteristic time of underthrusting	$\tau_{underthrust}$		Myr
Péclet number	Pe		
Magmatic thickening rate	M		km Myr <sup>-1</sup>

the lower crust,  $C_p(T)$  is temperature-dependent heat capacity, and F is melt fraction. The temperature-melt fraction relationship  $(\partial F/\partial T)$  is constrained using a MELTS-modeled phase change for a lower crust composition (see Section 2.3). Parameters used in the model are listed in Table 1. Equation 1 can be rearranged to:

$$\frac{\partial T}{\partial t} = \frac{\partial}{\partial z} \left[ \kappa'(T) \frac{\partial T}{\partial z} \right]$$
 (2)

where  $\kappa'(T)$  is the equivalent diffusivity taking latent heat into account (e.g., Lee et al., 2015b):

$$\kappa'(T) = \frac{\kappa(T)}{1 + \frac{L}{C_p(T)} \frac{\partial F}{\partial T}}$$
(3)

It is noted that  $\kappa'(T) < \kappa(T)$  since the denominator in Equation 3 is larger than 1. Implicit finite difference method and Picard iteration are used to solve the nonlinear heat equation (Equation 2). The MATLAB script used for the numerical model is included in the supporting information.

### 2.2. Effects of Temperature-Dependent Diffusivity and Latent Heat

Studies have shown that rock thermal diffusivity decreases rapidly with increasing temperature (Mottaghy et al., 2008; Vosteen & Schellschmidt, 2003). Whittington et al. (2009) shows that the thermal diffusivity of crustal rocks near and above Moho temperatures is about  $0.5 \times 10^{-6}$  m<sup>2</sup> s<sup>-1</sup>, which is approximately half its

YANG ET AL. 4 of 19

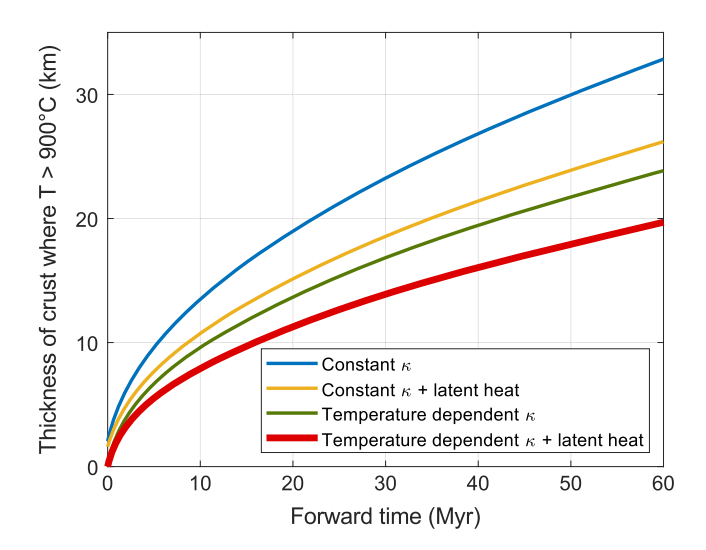


**Figure 3.** Temporal evolution of the underthrusted lower crustal slab showing the propagation of the 900°C isotherm. Inclusion of temperature-dependent diffusivity and latent heat significantly reduces the rate of heat transfer

value at temperatures on Earth's surface. The temperature dependence of diffusivity effectively slows conductive heat transfer within the underthrusting crust, thus reducing the rate of partial melting.

The effects of the temperature dependence of thermal diffusivity and latent heat are illustrated in Figure 3. In the half-space heating model, a column of initially isothermal  $600^{\circ}$ C crust is exposed at one end to mantle temperatures of  $1100^{\circ}$ C. By tracking the propagation of the  $900^{\circ}$ C isotherm, heating of the rock column is inhibited when the temperature dependency of thermal diffusivity or the effect of latent heat is applied. The combined effects of temperature-dependent thermal diffusivity and latent heat drastically slows down the rate of thermal conduction by a factor of  $\sim 3$  for the given scenario.

# 2.3. Partial Melting of Lower Crust and Formation of Arc Root

To obtain the temperature-melt fraction relationship needed for the calculation of latent heat, we use the MELTS thermodynamic algorithm (Ghiorso & Sack, 1995) to constrain the temperature-melt fraction relationship  $(\partial F/\partial T)$  during partial melting. For our generalized model of continental arc systems, we adopt the temperature-melt fraction relationship using the global average lower crust composition (Rudnick & Gao, 2003). The MELTS calculations were performed at 1.5 GPa

(lithostatic pressure at  $\sim$ 55 km depth using crustal density of 2,800 kg/m³) and a temperature range of 600°C–1300°C to mimic the conditions at which the underthrusting crust undergoes partial melting. Detailed MELTS setup and parameters are presented in the supporting information.

The global average lower crust used in the model is of mafic composition with a silica content of 52 wt. %. To investigate the effects of water during partial melting of the underthrusting lower crust, our experiments were performed assuming a range (1, 1.5, and 2 wt. %) of  $H_2O$ . The bulk source rock composition is listed in the MELTS setup file in the supporting information. Residual phase diagram and melt silica content for 1, 1.5, and 2 wt. % of  $H_2O$  is presented in Figure 4.

Ducea (2002) and Ducea et al. (2020) argue that the Sierra Nevada granitoids (arc magma) and the pyroxenite xenoliths (arc root) are complementary melts and residues, respectively, resulting from partial melting of mafic, amphibolitic lower continental crust, with 0.1–0.5 melt fractions. Segregation of partial melt in the lower crust begins at the melt connectivity transition, where isolated melt pockets coalesce to form an interconnected melt network along the grain boundaries, enabling melt permeability at the source region and allowing melt to migration (e.g., Rosenberg & Handy, 2005; Sawyer, 1994). We assume partial melting of the lower crust continues until melt of intermediate composition is extracted, and dense restitic minerals (mostly garnet and pyroxenite) are left over. We define a critical melt fraction ( $F_{crit}$ ) as the degree of partial melting of underthrusted lower crust required to generate melt of intermediate composition.

The value of critical melt fraction is set to  $F_{\rm crit}=0.25$  because of the following reasons. First, at  $F_{\rm crit}=0.25$ , for all three choices of different water contents, the restite consists of mostly garnet and pyroxene, an eclogitic assemblage (Figure 4). This is similar to the characteristic mineralogy of the Sierra Nevada arc root (Ducea & Saleeby, 1996; Ducea, 2002). The melt produced at  $F_{\rm crit}=0.25$  is also granitic with a silica content of 65–70 wt. %. Second, after testing different  $F_{\rm crit}$  values ranging from 0.1 to 0.5, we found  $F_{\rm crit}$  of 0.25 provides the maximum amount of melt produced in 50 Myr timescales because a higher  $F_{\rm crit}$  corresponds to a higher temperature ( $T_{\rm crit}$ , defined in the following paragraph) that makes melting more difficult (see Figure S1). Third, the 0.25 melt fraction is also similar to that estimated in Betic Cordilleran orogen in southern Spain, based on Mn growth zoning in peritectic garnets (0.3 melt fraction; Yu & Lee, 2016). In our 1-D model,  $F_{\rm crit}$  also equals the thickness ratio of total partial melt generated to the underthrusted lower crust. An eclogitic arc root forms after extraction of intermediate melt (Ducea, 2002). With  $F_{\rm crit}=0.25$ , the thickness of the arc root resulting from partial melting is three times the thickness of the extracted melt. This arc root could exist throughout an arc's evolution, but it may also founder into the mantle due to gravitational instability (e.g.,

YANG ET AL. 5 of 19

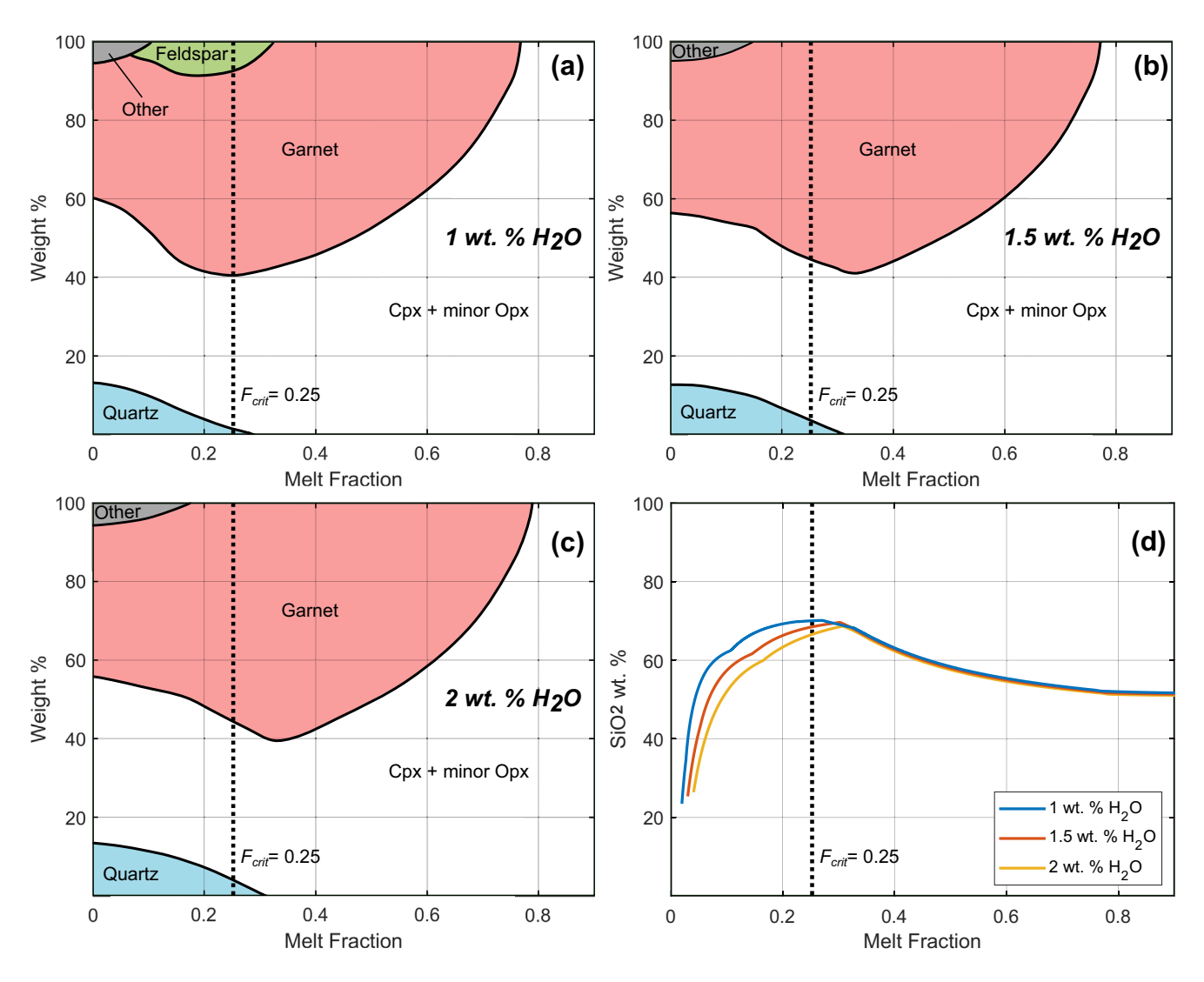


Figure 4. MELTS partial melting results of global average lower crust composition (Rudnick & Gao, 2003) containing 1, 1.5, and 2 wt. %  $H_2O$ . (a–c) Phase diagram of residual mineral weight percent as a function of melt fraction. (d) Silica content in melt versus melt fraction.  $F_{crit}$  is the critical melt fraction ( $F_{crit} = 0.25$  means 25% partial melting).

Arndt & Goldstein, 1989; Lee, 2014). The eclogitic root undergoes no further melting because of the high solidus (>1300°C) for eclogitic compositions (Mallik & Dasgupta, 2012).

Finally, we define a critical temperature ( $T_{\rm crit}$ ) corresponding to  $F_{\rm crit}=0.25$  (Figure 5). Increased water content lowers the solidus as well as  $T_{\rm crit}$ , making partial melting more rapid. When the lower crust contains 1.5 and 2 wt. %  $H_2O$ , the  $T_{\rm crit}$  is lowered by 72°C and 108°C, respectively, compared to the 1 wt. %  $H_2O$  case (Figure 5).

### 2.4. Models of the Underthrusting Rate

Underthrusting of the retro-arc lower crust is initiated at the start of the simulation and terminated when the lower crust intercepts the cold mantle lithospheric wedge beneath the fore-arc region (Figure 2). Based on geological estimates of total retro-arc crustal shortening (e.g., Sevier thrust belts and hinterland shortening) associated with the Cretaceous Sierra Nevada arc, the average upper crust shortening rate is  $\sim$ 5 km/Myr and is more or less constant from  $\sim$ 120 to 80 Ma (DeCelles, 2004; Yonkee & Weil, 2015). If the lower crust experienced the same amount of shortening, the average underthrusting rate of the lower crust would also be  $\sim$ 5 km/Myr.

YANG ET AL. 6 of 19

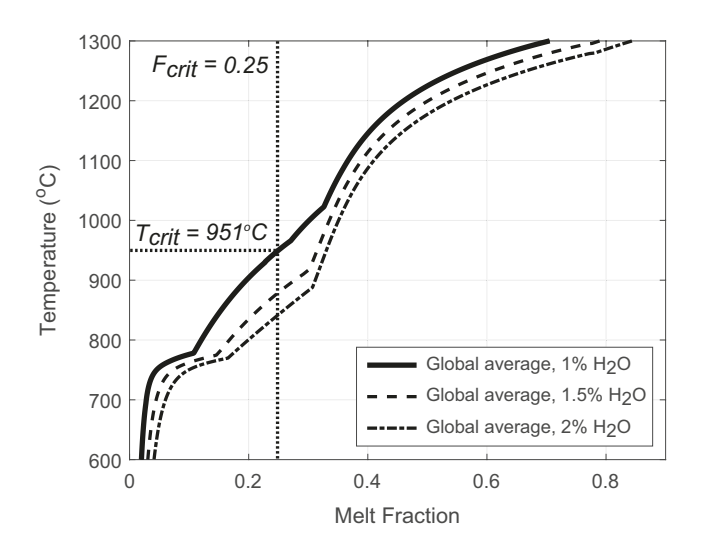


**Figure 5.** Temperature versus melt fraction diagram for the global average lower crust composition (Rudnick & Gao, 2003) constrained by MELTS. Different water content in weight percent is presented.  $T_{\rm crit}$  is the temperature corresponding to  $F_{\rm crit}=0.25$ .

# 2.5. Magmatic Thickening Rate and Volume of Arc Magma

Melt volume is calculated via the product of underthrusting distance x(t), the thickness of the 1-D crustal column undergoing partial melting and melt extraction z(t), the along strike arc length (l), and the critical melt fraction  $(F_{crit})$  (Equation 4). z(t) is determined based on the result of the 1-D half-space heating model where the temperature exceeds a critical temperature  $(T_{crit})$  (Figure 5). We then apply z(t) laterally across the entire underthrusted crust to obtain the estimated magma volume (Equation 4):

$$V(t) = A \cdot l \cdot F_{\text{crit}} = x(t) \cdot z(t) \cdot l \cdot F_{\text{crit}}$$
(4)

where A is the melt area in the 2-D profile. Since v(t) is underthrusting rate (Equation 5), we have

$$x(t) = \int_{0}^{t} v(t)dt \tag{5}$$

We assume the arc magma generated through partial melting is uniformly distributed along the width of the arc. To calculate the magmatic thickening rate M(t), we take the time derivative of Equation 4 and divide it by the 2-D surface area of the arc  $(w \cdot l)$  (Equation 6):

$$M(t) = \frac{dV}{dt} \cdot \frac{1}{wl}.$$
 (6)

Since we do not solve thermal diffusion in 2-D, the melt area is slightly overestimated. The actual area of melt can be constrained between the upper limit of  $x \cdot z$  (the value we used in the model) and the lower limit of  $\frac{2}{3}x \cdot z$ . The lower limit is calculated via integrating the area of melt assuming only 1-D vertical thermal diffusion (see Figure S2). In this sense, our simplified method overestimates the melt volume by no more than  $\sim$ 30%. This approach works together with other assumptions in our model (e.g., constant mantle temperature) yielding the upper limit of magma generation during the underthrusting process.

#### 2.6. Model Limitations

Our numerical model provides first-order estimates on the total magma volume and magmatic thickening rate associated with the underthrusting process. While we focused on the process of retro-arc underthrusting, the results from our generic model is applicable to fore-arc underthrusting as well. However, this model is simplified, and there are several limitations: (1) Our approach does not account for the refrigerating effect on the mantle (Chin et al., 2015) due to the magmatic and tectonic thickening of arc crust (Cao et al., 2016b; Karlstrom et al., 2014; Lee et al., 2015a) and derthrusting of a relatively colder crust. The refrigerating effect could gradually lower the temperature of the mantle, hamper heating of the underthrusting crust. (2) We assume all melts are added to the arc crust as soon as they are generated. There is no lag time associated with melt transport, and the physical processes of magma ascent and emplacement (e.g., Cao et al., 2016a; Rummel et al., 2020) are not considered. (3) Magma advection as dikes or diapirs are not included. Advection could promote heat transfer by increasing the equivalent thermal diffusivity (e.g., England et al., 2007; Jaupart & Mareschal, 2010); therefore, it may boost the rate of heat transfer within the underthrusted crust. In Section 4.2 of the discussion, we parameterized thermal advection in a simple, semi-quantitative manner. More advanced modeling on the actual physical processes of magma advection is needed in future studies. (4) We do not include any spatial or temporal focusing processes which could boost the local magmatic thickening rate. For example, the center of the arc front may receive a higher melt flux via arc axial focusing relative to the peripheral arc region (Ardill et al., 2018). (5) Our model does not include the dynamics of arc root foundering, mantle flow upwellings, and subsequent partial melting of the lower crust. Some of the above aspects may have competing effects on melt generation and would require more comprehensive 2-D/3-D modeling.

YANG ET AL. 7 of 19

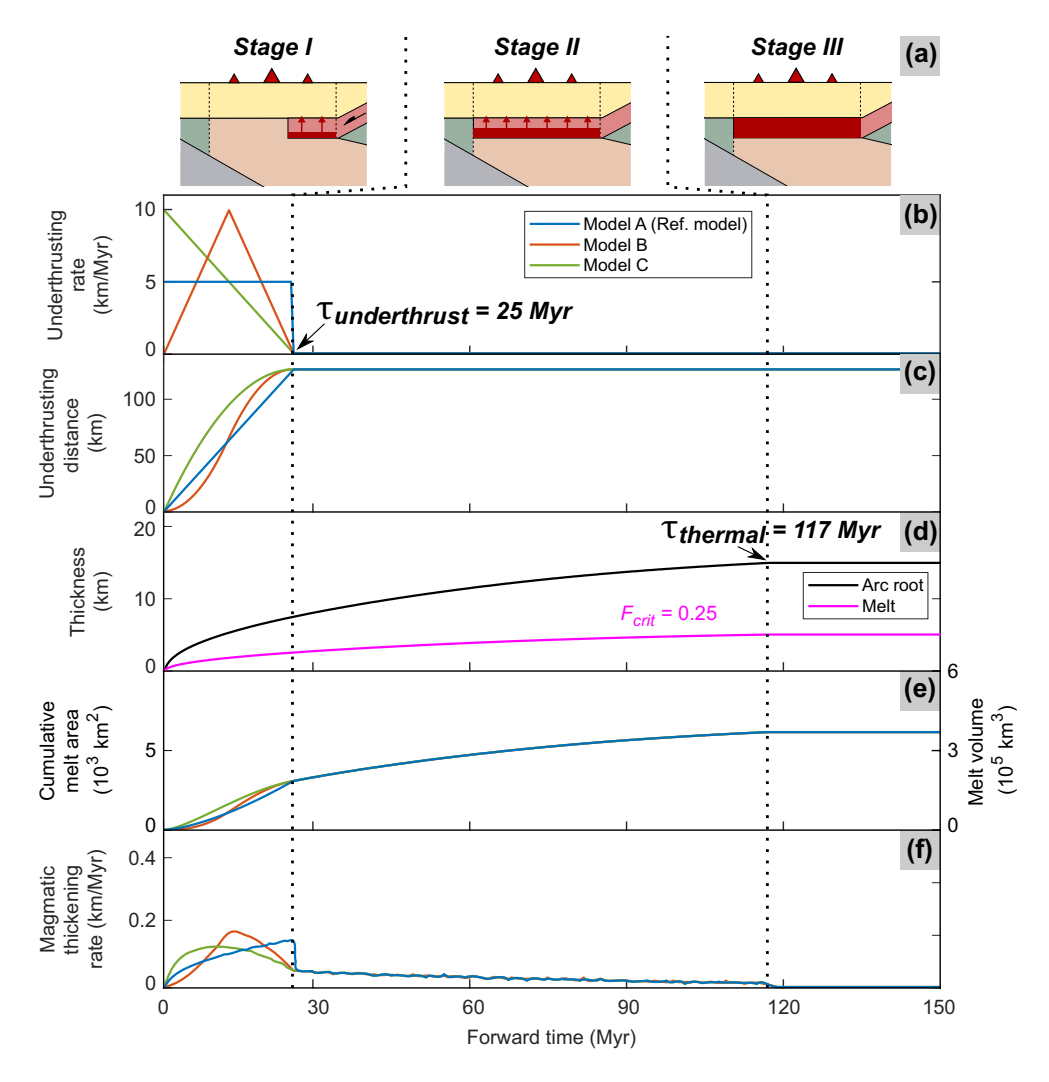


**Figure 6.** Numerical simulation results of Case 1 with 1 wt. % water showing the temporal evolution of three models with different underthrusting rates. (a) The model results are categorized into three stages based on underthrusting of the lower crust. The red part of the underthrusted crust refers to the area undergoing partial melting and melt extraction. (b) Time-dependent underthrusting rate. (c) Total underthrusting distance. (d) Thickness of arc root generated via partial melting and cumulative melt thicknesses for  $F_{\rm crit} = 0.25$ . (e) Cumulative 2-D melt area and 3-D melt volume for arc width w = 125 km and arc length l = 600 km. (f) Magmatic thickening rate or volumetric flux.

#### 3. Results

We present two results of numerical simulations with different water contents. In Figure 6, the water content of the underthrusted crust is set to 1 wt. %, while Figure 7 corresponds to a water content of 2 wt. % to demonstrate the effect of water on the melt generation rate. For each simulation, we tested three models of underthrusting rate. The reference model (Model A) has a constant rate of 5 km/Myr representing the most likely case for the Cretaceous Sierra Nevada arc (e.g., Yonkee & Weil, 2015). Model B has a linearly increasing and decreasing rate which steadily increases to 10 km/Myr during the first half of underthrusting, then decreases to 0 during the second half. Model C has a linear decreasing rate where  $\nu=10$  km/Myr at the start and decreases to 0 at the end. The purpose of the time-dependent rates in Models B and C is to investigate how underthrusting rate influences the magmatic thickening rate. These models (Models B and C) do not reflect the geological constraints on the underthrusting rate. For each case, the average underthrusting rate is 5 km/Myr. To facilitate discussion, we defined two characteristic times. The characteristic time of underthrusting ( $\tau_{\rm underthrust}$ ) is the timescale of active underthrusting (the ratio between the given arc width, 125 km, and average underthrusting rate).  $\tau_{\rm underthrust}$  is 25 Myr in all models. We also defined the characteristic

YANG ET AL. 8 of 19

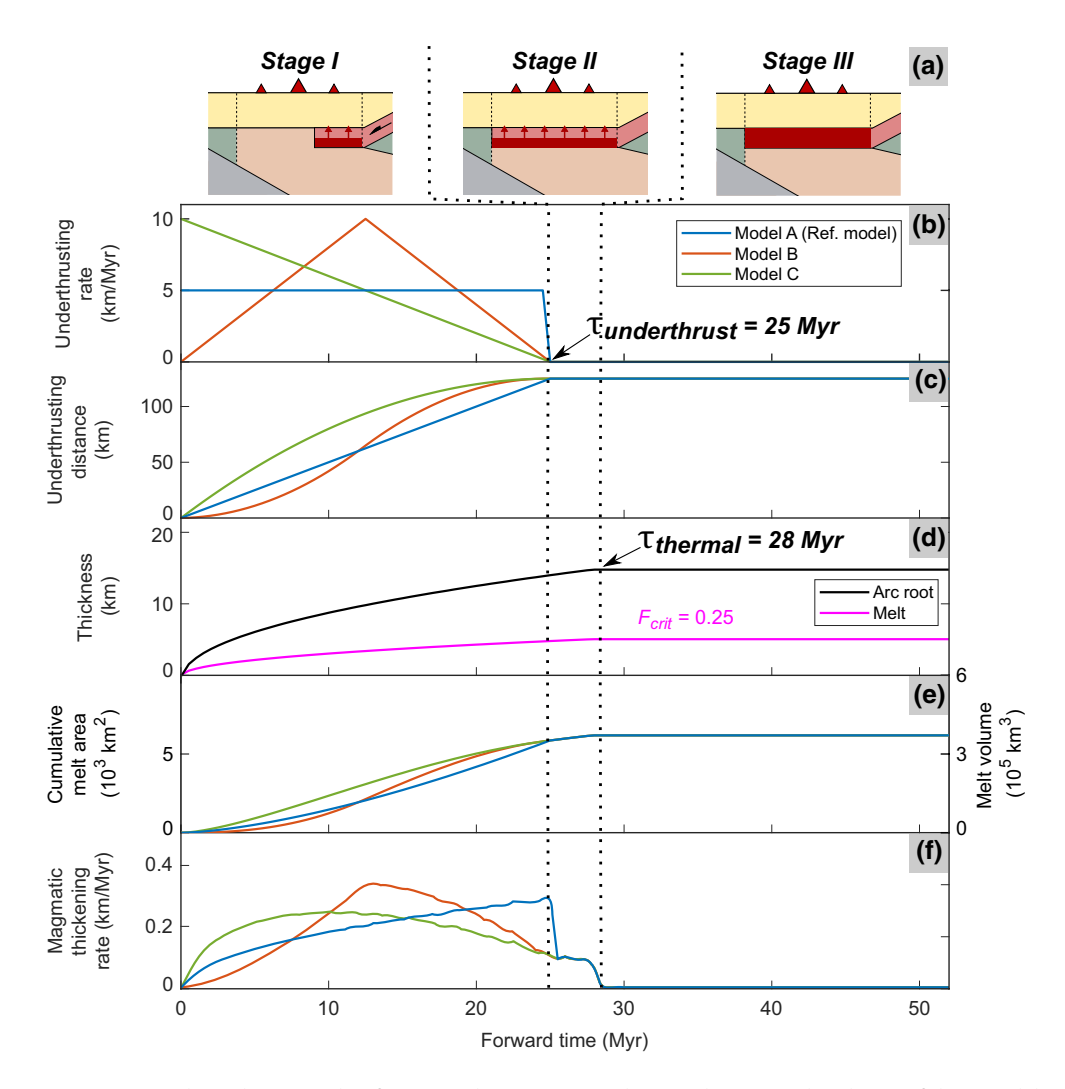


**Figure 7.** Numerical simulation results of case 2 with 2 wt. % water showing the temporal evolution of three models with different underthrusting rates. Except for the increased water content, all other parameters are unchanged to illustrate the effect of water on melt generation. (a) The model results are categorized into three stages. The red part of the underthrusted crust refers to the area undergoing partial melting and melt extraction (see text for detailed explanation). (b) Time-dependent underthrusting rate. (c) Total underthrusting distance. (d) Thickness of arc root generated via partial melting and cumulative melt thicknesses for  $F_{\rm crit} = 0.25$ . (e) Cumulative 2-D melt area and 3-D melt volume for arc width w = 125 km and arc length l = 600 km. (f) Magmatic thickening rate or volumetric flux.

time of heat transfer ( $\tau_{thermal}$ ) as the time needed to complete the partial melting of the underthrusted crust along its vertical dimension.

# 3.1. Case 1 With 1 wt. % Water

The results of Case 1 containing 1 wt. % water can be categorized into three stages. Below, we summarize the results for each stage.

# 3.1.1. Stage I

Active underthrusting with vertical growth of the partial melt layer ( $t < \tau_{\rm underthrust}$ ). The lower crust begins underthrusting from the retro-arc direction, and partial melting occurs. During this stage, melt generation is sustained by both lateral underthrusting of the lower crust and vertical growth of the partial melt layer. Stage I ends when the entire sub-arc mantle is occupied by the crustal slab, and it intercepts the mantle wedge beneath the forearc (Figure 2).

YANG ET AL. 9 of 19



Models of different underthrusting rates (Figure 6b) result in slightly different underthrusting distances during this stage, though the final underthrusting distance of 125 km is the same for all cases (Figure 6c). The cumulative melt thickness increases as the isotherm  $T_{\rm crit}$  vertically propagates upward through the crustal column (Figure 6d, pink curve). The thickness scales with  $\sim t^{1/2}$  during this stage because the melt thickness is controlled by thermal diffusion and is independent of the underthrusting rate. Cumulative melt thickness and melt volume also increases with time (Figure 6e). At the end of Stage I, melt volume reaches  $2 \times 10^5$  km<sup>3</sup>.

The magmatic thickening rate is sensitive to the underthrusting rate (Figure 6f). For the reference Model A with the constant 5 km/Myr underthrusting rate, the magmatic thickening rate slowly climbs to a maximum of  $\sim$ 0.15 km/Myr when underthrusting ends. For Model B with linearly increasing and decreasing rates, the magmatic thickening rate mimics the temporal pattern of the underthrusting rate. The maximum thickening rate of  $\sim$ 0.2 km/Myr is achieved in the middle of the stage when the underthrusting rate reaches a peak of 10 km/Myr. For Model C with a linear decreasing rate, the maximum thickening rate of  $\sim$ 0.1 km/Myr occurs within the first half of Stage I, before 10 Myr.

# 3.1.2. Stage II

Vertical growth of the partial melt layer after underthrusting terminates at 25 Myr ( $\tau_{underthrust} < t < \tau_{thermal}$ ). Partial melting is sustained by the upward propagation of the isotherm  $T_{crit}$ . Even without additional underthrusting lower crust, the cumulative melt area and volume still increase during Stage II but at a slower rate than Stage I (Figure 6e). This behavior is also reflected in the magmatic thickening rate, which decreases to  $\sim 0.05$  km/Myr (Figure 6f). Stage II ends when the entire vertical column of the underthrusted slab has undergone partial melting. In other words, the end of Stage II is marked by the  $T_{crit}$  isotherm reaching the top of the 20 km-thick underthrusted slab ( $t = \tau_{thermal}$ ).  $\tau_{thermal}$  is 117 Myr in the Case 1 simulation and Stage II lasts 92 Myr (117 - 25 = 92 Myr). Once Stage II is complete, no additional melt can be produced because the entire slab has undergone partial melting. At the end of Stage II, the maximum melt volume has reached  $3.75 \times 10^5$  km³, and the arc root is completely formed.

#### 3.1.3. Stage III

Cessation of partial melting in the underthrusted crust ( $t > \tau_{\text{thermal}}$ ). One complete underthrusting-partial melting process in Case 1 takes 117 Myr which equals  $\tau_{\text{thermal}}$ .

#### 3.2. Case 2 With 2 wt. % Water

Similar to Case 1, we defined the same three stages in Case 2, with the increased water content (2 wt. % H<sub>2</sub>O). In this case, partial melting along the vertical dimension of the underthrusted crust is completed shortly after lateral underthrusting terminates. Therefore, the duration of Stage II (3 Myr) is much shorter in Case 2 (3 Myr compared to 92 Myr in Case 1).

#### 3.2.1. Stage I

Active underthrusting with vertical growth of the partial melt layer ( $t < \tau_{underthrust}$ ). Compared to Case 1, the magmatic thickening rate is higher in Case 2. The three models achieve different maximum rates at different times: (1) magmatic thickening rate of ~0.3 km/Myr at the end of Stage I in Model A; (2) ~0.35 km/Myr at 12.5 Myr when the peak underthrusting rate of 10 km/Myr is reached in Model B; and (3) ~0.25 km/Myr around 10 Myr in Model C. Stage I ends when the entire sub-arc mantle is occupied by the crustal slab, and it intercepts the mantle wedge beneath the forearc (Figure 2).

# 3.2.2. Stage II

Vertical growth of the partial melt layer after underthrusting terminates at 25 Myr ( $\tau_{underthrust} < t < \tau_{thermal}$ ). During this stage, partial melting is sustained by the upward propagation of the isotherm  $T_{crit}$ . Without the underthrusting of the lower crust, we observe a decrease in magmatic thickening rate to  $\sim$ 0.1 km/Myr (Figure 7f), roughly twice the value shown in Case 1. Since the characteristic time of heat transfer within the underthrusted crust ( $\tau_{thermal}$ ) is 28 Myr, Stage II in this case only lasts for 3 Myr (28 - 25 = 3 Myr). No additional melt can be produced after the end of Stage II because the entire underthrusted crust has undergone partial melting. At this point, the maximum melt volume of  $3.75 \times 10^5$  km³ is reached for an assumed

YANG ET AL. 10 of 19

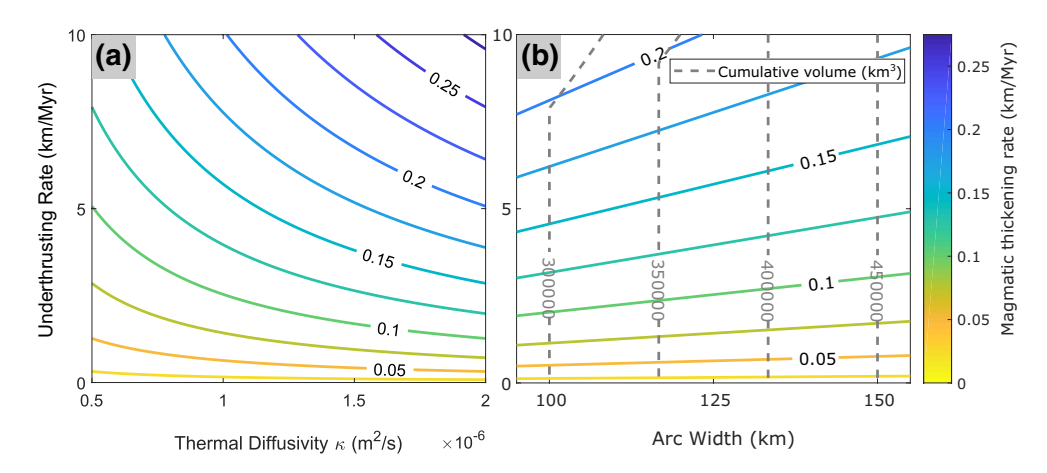


Figure 8. Steady-state results showing dependency of magmatic thickening rate (colored contours) with various input parameters. (a) Magmatic thickening rate as a function of underthrusting rates and thermal diffusivity with fixed arc width w=125 km.  $F_{\rm crit}=0.25$  is used. (b) Magmatic thickening rate as a function of arc width and underthrusting rate. Constant thermal diffusivity  $\kappa=10^{-6}$  m²/s and  $F_{\rm crit}=0.25$  is used. Cumulative melt volume for a given arc width is shown in dashed gray lines for arc length l=600 km. Kinks in the dashed gray line of melt volume appear when the underthrust rate is high and arc width is small which results in incomplete partial melting when the underthrusting stops ( $\tau_{\rm thermal} > \tau_{\rm underthrust}$ ).

continental arc whose width w = 125 km and length l = 600 km (Figure 7e) and the formation of the arc root for the entire underthrusted crust is complete.

#### 3.2.3. Stage III

Cessation of partial melting in the underthrusted crust ( $t > \tau_{\text{thermal}}$ ). The complete underthrusting-partial melting process in Case 2 takes 28 Myr which equals  $\tau_{\text{thermal}}$ .

### 4. Discussion

#### 4.1. Scaling Analysis: Steady-State Model

A simple, idealized steady-state model is presented to illustrate the scaling relationships among the parameters controlling arc magma generation as a result of partial melting (Figure 8). This scaling model does not include the effects of latent heat nor water in the lower crust, and thermal diffusivity is treated as a constant ( $\kappa$ ). At steady-state, the lower crust is underthrusted into the sub-arc mantle at a constant rate  $\nu$ , and arc root is readily removed. Using the characteristic thickness of the conductive thermal boundary ( $\sqrt{\kappa t}$ ) and a critical fraction ( $F_{\rm crit}$ ), we obtain a melt thickness of (Equation 7):

$$z = F_{\text{crit}} \sqrt{\kappa t} \tag{7}$$

In this scaling analysis, the characteristic time of underthrusting,  $\tau_{underthrust}$ , is given by the quotient of arc width w and underthrusting rate v (Equation 8):

$$\tau_{\text{underthrust}} = \frac{w}{v} \tag{8}$$

The magmatic thickening rate M of the lower crust during steady-state conditions can be obtained by taking the time derivative of z (Equation 7) and replacing t with  $\tau_{\text{underthrust}}$  (Equation 9):

$$M = \frac{dz}{dt} = \frac{1}{2} \cdot F_{\text{crit}} \sqrt{\frac{\kappa v}{w}}.$$
 (9)

Finally, the total volume of arc magma generated within the characteristic time of underthrusting can be calculated by the product of the arc width w, the along strike arc length l, and the melt thickness (z) at time  $\tau_{\text{underthrust}}$  (Equation 10):

YANG ET AL. 11 of 19

$$V = w \cdot l \cdot z = w \cdot l \cdot F_{\text{crit}} \sqrt{\frac{\kappa w}{v}}.$$
 (10)

Figure 8 illustrates the magmatic thickening rate and the total magma volume as a function of the underthrusting rate, the thermal diffusivity, and the arc width using  $F_{\rm crit}=0.25$ . At steady-state, the magmatic thickening rate is positively correlated with the underthrusting rate and thermal diffusivity (Figure 8a) and inversely correlated with arc width (Figure 8b). In comparison, cumulative melt volume is largely a function of arc width. A larger arc width enables more material to be underthrusted, resulting in greater cumulative melt volume.

The magmatic thickening rate only weakly depends on the arc width within a reasonable range of widths (100–150 km) (Figure 8b).

The upper bound estimates of magmatic thickening rate and cumulative melt volume correspond to an unlikely scenario of  $F_{\rm crit}=1$ , in which the underthrusted lower crust is completely melted and all materials are added to the arc crust. Using values representative of the Sierra Nevada arc where l=600 km, w=125 km, and v=5 km/Myr, the magmatic thickening rate is 0.6 km/Myr or  $\sim$ 2 AU equivalent. Also, for the  $F_{\rm crit}=1$  case, one complete underthrusting event yields a cumulative melt volume of  $1.5\times10^6$  km³. This melt volume is 67% of the original arc crust (125 km width  $\times$  600 km length  $\times$  30 km depth). The 0.6 km/Myr thickening rate and magma volume of  $1.5\times10^6$  km³ are close to the lower end of the estimated values of the Cretaceous flare-up event in the entire Sierra Nevada ( $M=\sim0.6-1$  km/Myr and  $V=\sim1-3\times10^6$  km³) (e.g., Cao & Paterson, 2016; Ratschbacher et al., 2019). However, only a portion of the crust undergoes partial melting; the rest becomes residue. In the case of  $F_{\rm crit}=0.25$  (Figure 8), the magmatic thickening rate and cumulative melt volume will be reduced by a factor of 4, resulting in M=0.15 km/Myr or 0.5 AU equivalent and  $V=3.7\times10^5$  km³. Volumetrically, it is less than 20% of the original arc crust. This simple scaling analysis shows that the volume of magma generated by partial melting of the crust and the magmatic thickening rate cannot suffice flare-up events. Magma from additional sources is required to reach the estimated magma thickening rate and volume.

#### 4.2. Effects of Water and Heat Advection

Higher water content in the underthrusted crust lowers the solidus as well as the  $T_{\rm crit}$  of the crust, increasing the rate of partial melting (Figure 5). For the top row in Figure 9 (A1, A2, and A3), where the water content increases from left to right, there is an increase in peak magmatic thickening rate corresponding to higher water content. The higher water content also reduces the  $\tau_{\rm thermal}$ , enabling faster partial melting along the vertical dimension of the underthrusted crust. However, the magmatic thickening rate in the highest water content case is still much lower than the estimated thickening rate during a flare-up. For the reference model A (blue curves in A2 and A3 of Figure 9), the addition of water only boosts the peak magmatic thickening rate to  $\sim$ 0.3 km/Myr. In terms of magma volume, the total amount of melt produced from partial melting of the underthrusted crust remains unchanged because it is capped by the size of the underthrusted crust and the given critical melt fraction. Since  $\tau_{\rm thermal}$  corresponding to the 1 wt. % water case is  $\sim$ 117 Myr, only a portion of the total magma volume is released in timescales of  $\sim$ 30 Myr, typical for an arc flare-up (Figure 6). Whereas for 1.5 and 2 wt. % water,  $\tau_{\rm thermal}$  is much shorter (30 and 28 Myr, respectively, Figure 9); thus, the maximum magma volume is reached much faster with increased water content.

Advective heat transfer (e.g., diking) from mantle basalts intruding into the lower crust could heat the crust in addition to thermal conduction. The intruding basalts will thus in turn play an important role in increasing the magma production rate. Magma advection via diking are difficult phenomena to implement even in advanced 2-D or 3-D models because the processes depends on many complex, dynamic processes, and parameters such as rock rheology, melt transport, phase transition, and dike formation mechanisms (e.g., Cao et al., 2016a; Liang & Parmentier, 2010; Rummel et al., 2020). While others have quantitatively assessed the process of advective magma transport and the thermal impact of mantle melt on the lithosphere using sophisticated, two-phase flow dynamics (Keller et al., 2013; Rees Jones et al., 2018). We acknowledge that our simple thermal-kinematic model is incapable of simulating the actual processes of magma advection. Instead, we adopted an "amplification factor of thermal diffusivity" to quantify the thermal effect of advection in addition to conduction.

YANG ET AL. 12 of 19

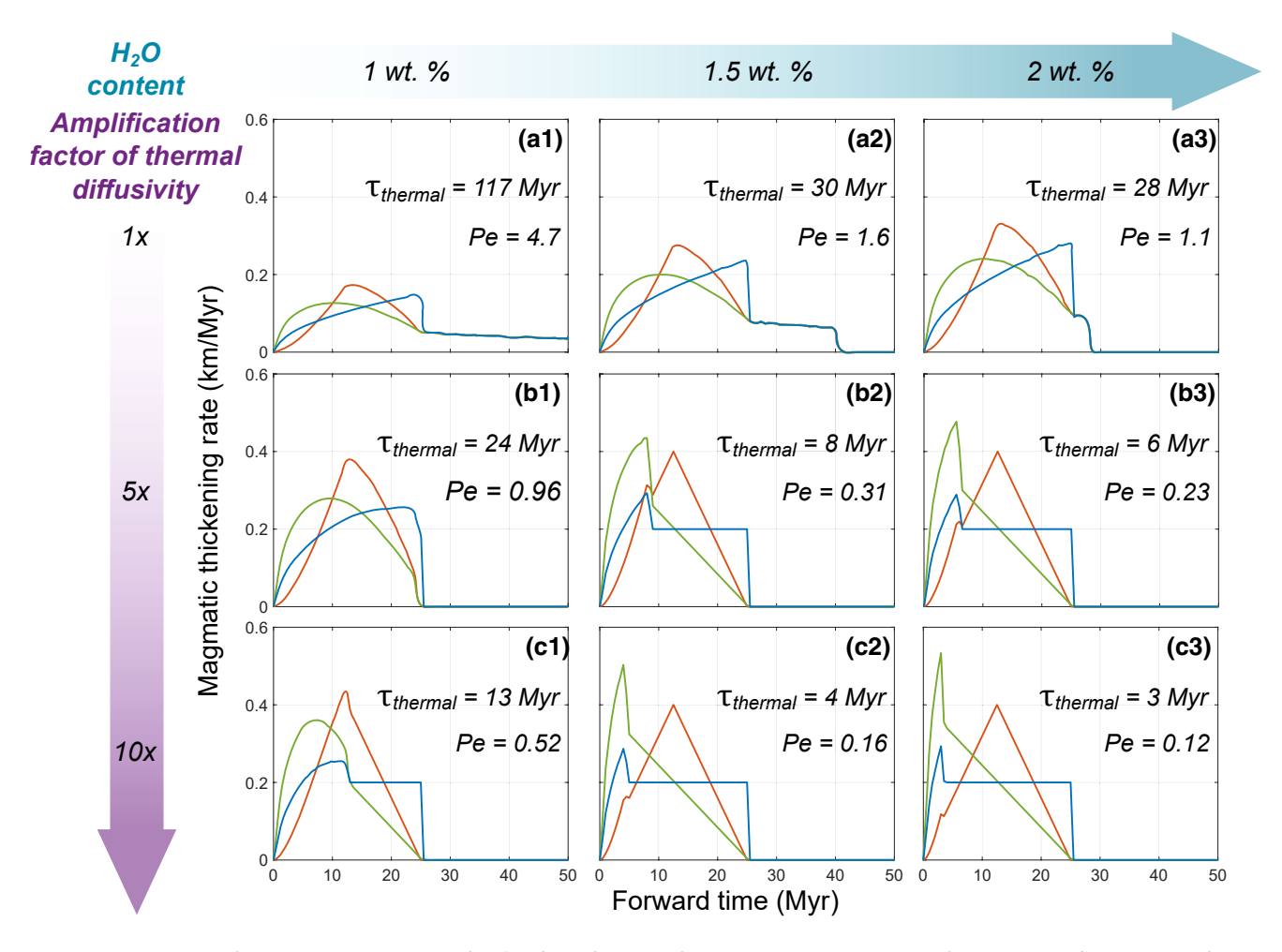


Figure 9. Simulation results of magmatic thickening rate (km/Myr) as a function of time. Multiple combinations of water content (horizontal row) and amplification factor of thermal diffusivity (vertical column) are presented. Colored lines represent the three underthrusting rate models: Blue line (Reference Model) is the constant underthrusting rate of 5 km/Myr. Red and green lines represent cases having time-dependent underthrusting rate. Red line is a linearly increasing and decreasing rate which steadily increases to 10 km/Myr during the first half of underthrusting, then decreases to 0 during the second half. Green line is a linear decreasing rate from 10 km/Myr at the start to 0 at the end. All three rate models have a underthrusting duration ( $\tau_{underthrust}$ ) of 25 Myr.  $\tau_{thermal}$  varies in different models, and Pe is the Péclet number defined as the ratio between  $\tau_{thermal}$  and  $\tau_{underthrust}$ .

In addition to the original temperature-dependent thermal diffusivity with latent heat included, we tested 5X and 10X amplification factors of thermal diffusivity in our models (Figure 9). The 5X and 10X factors are based on the following argument. Karakas and Dufek (2015) used stochastic modeling of repetitive basaltic magma emplacement from the mantle into the lower crust as dikes and sills. Their simulation results show a temperature perturbation with a vertical length scale of  $\sim\!20$  km emerging within 1–2 Myr. Using the characteristic timescale of thermal diffusion, we can infer an equivalent thermal diffusivity ( $\kappa_{eq}$ ) using Equation 11.

$$\kappa_{\rm eq} = \frac{x^2}{t} \tag{11}$$

where t is time and x is length of the crustal temperature perturbation in this case. The resulting  $\kappa_{eq} = 10^{-5}$  m<sup>2</sup>/s if t = 1 Myr and x = 20 km. If t = 2 Myr,  $\kappa_{eq} = 5 \times 10^{-6}$  m<sup>2</sup>/s. These values are 10 and 5 times the reference thermal diffusivity ( $\kappa = 10^{-6}$  m<sup>2</sup>/s), respectively.

The effect of such parameterized thermal advection is illustrated in Figure 9. As expected, the magmatic thickening rate is increased due to a faster vertical thermal propagation rate, reducing the time needed to heat the underthrusted crust for partial melting. Since  $\tau_{thermal}$  is inversely correlated with thermal diffusivity,

YANG ET AL. 13 of 19



as the amplification factor of thermal diffusivity increases,  $\tau_{thermal}$  becomes shorter. However, even with water added to the system (2 wt. %) and a 10X amplification factor (C3 in Figure 9), the magmatic thickening rate is still below 0.3 km/Myr for the constant underthrusting case (blue curve, the most likely underthrusting velocity profile). This value is too low to qualify as an arc flare-up. In some cases (e.g., B3, C2 in Figure 9), brief pulses of magmatic thickening rates exceeding 0.4 km/Myr appear in the early stage ( $\sim$ 5 Myr) of the simulation. These pulses are due to the initial rapid melt generation of the underthrusted crust as it enters the sub-arc mantle in high  $\kappa_{eq}$  (or high amplification factor) and water-rich cases. The magmatic thickening rates then return to lower values sustained by the lateral underthrusting.

### 4.3. Controls on the Magma Volume and Magmatic Thickening Rate

The total cumulative volume of arc magma generated through partial melting of underthrusted crust is limited by the thickness of the underthrusted crust for a given critical melt fraction ( $F_{crit}$ ). Results of the numerical simulation suggest that for a continental arc analogous to the Sierra Nevada arc, in pure conduction and 1 wt. % water case, one underthrusting event produces a cumulative melt volume of  $3.75 \times 10^5$  km³, and 45% of this volume is generated by the end of Stage I (Figure 6e). This equates to roughly 2.3 km of magmatic thickening in the overriding crust within 25 Myr. The crust would thicken an additional 2.7 km during Stage II, from 25 to 117 Myr. In simulations having higher water content or higher diffusivity amplification factor (or higher  $\kappa_{eq}$ ), the maximum melt volume is generated within 30 Myr (Figure 9). The maximum melt volume estimate from numerical simulation ( $3.75 \times 10^5$  km³) is similar to the scaling analysis result ( $3.7 \times 10^5$  km³), both of which are much lower than the estimated magma volume ( $\sim 1-3 \times 10^6$  km³) during the Late Cretaceous Sierra Nevada flare-up (Cao & Paterson, 2016; Ratschbacher et al., 2019). The total volume of magma generated through partial melting is 13%–40% the estimated volume for a flare-up event.

Whether partial melting of the underthrusted lower crust is completed before or after underthrusting stops depends on the ratio between  $\tau_{\text{thermal}}$  and  $\tau_{\text{underthrust}}$ , in a similar form to the Péclet number (*Pe*):

$$Pe = \frac{\tau_{\text{thermal}}}{\tau_{\text{underthrust}}} \tag{12}$$

When Pe > 1, underthrusting is finished before the underthrusted crust undergoes complete partial melting for its entire thickness. The magmatic thickening rate is thus limited by the rate of vertical heat transfer, which is slower than the underthrusting rate (A1, A2 in Figure 9). When  $Pe = \sim 1$ , underthrusting is finished almost at the same time when the underthrusted crust goes through partial melting (A3, B1 in Figure 9). When Pe < 1, vertical heat transfer rate outpaces the underthrusting rate and the underthrusted crust experiences complete partial melting before underthrusting is finished. In this case, the magmatic thickening rate is limited by the lateral underthrusting process (e.g., B2, C1 in Figure 9). This effect can be seen where the magmatic thickening rate simply mimics the underthrusting rate in the later stage of the evolution. When  $Pe \ll 1$ , the magmatic thickening rate is essentially controlled by the underthrusting rate (e.g., B3, C2, C3 in Figure 9).

Results of both the scaling analysis and the numerical modeling demonstrate that the magmatic thickening rate strongly depends on the underthrusting rate (Figures 6, 7, and 9). This dependency is more apparent for the cases where  $Pe \ll 1$ . Such dependence of magmatic thickening rate on the underthrusting rate suggests that the observed bell-shaped magmatic flare-up signals defined by zircon age peaks (e.g., Paterson & Ducea, 2015) may necessitate a similar bell-shaped underthrusting rate through time (similar to the underthrusting rate in Model B). However, current estimates on how the underthrusting rate has changed with time does not support a bell-shaped profile of underthrusting rate with time. For example, the retro-arc shortening rate is fairly constant as we show in our reference model (Model A) (e.g., Yonkee & Weil, 2015). Thus, magma solely generated via underthrusting cannot produce the observed temporal pattern of a flare-up. Furthermore, the magmatic thickening rate (0.1–0.3 km/Myr) predicted in both the numerical reference model (Model A, blue curves in Figure 9) and the scaling analysis is significantly lower than observed values (0.6–1 km/Myr) during flare-ups in many Cordilleran arcs (e.g., Cao & Paterson, 2016; Jiang & Lee, 2017; Ratschbacher et al., 2019). The model predicted values are slightly below or similar to the baseline of arc magma thickening rate ( $\sim$ 0.3 km/Myr) from the mantle wedge (DeCelles et al., 2009; Reymer & Schubert, 1984).

YANG ET AL. 14 of 19

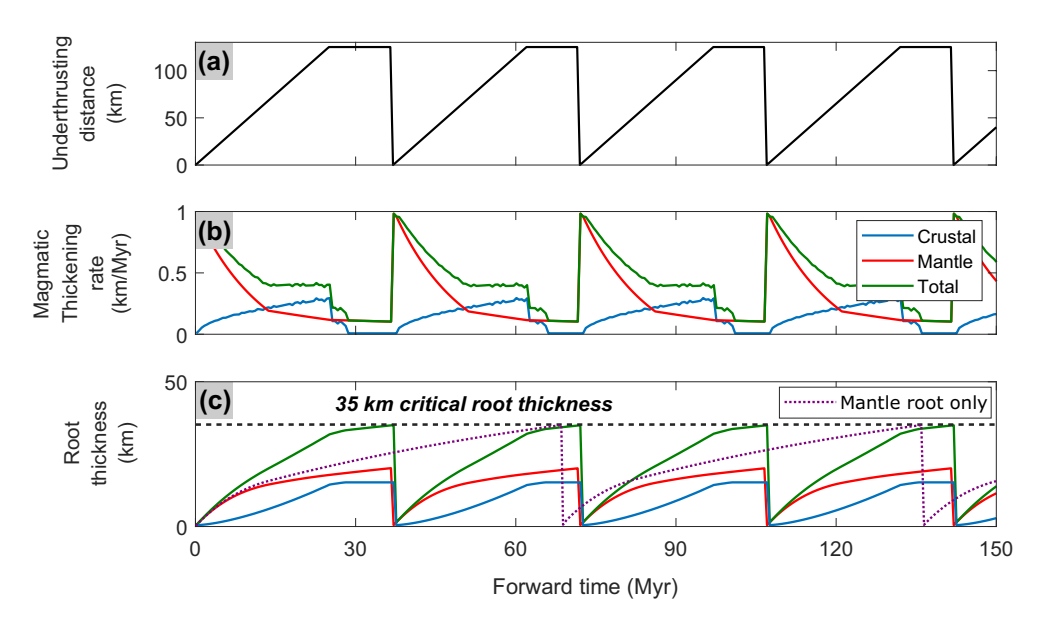


**Figure 10.** Modeling results of cyclic underthrusting and root foundering. (a) Lateral distance of the underthrusting lower crust. (b) Magmatic thickening rate sourced from the underthrusted crust (blue), mantle (red), and total (green). (c) Arc roots contributed by different processes. The horizontal black dashed line is an assigned critical thickness (35 km) for arc root to founder (e.g., Lee et al., 2015a). Purple line is mantle arc root only without the contribution of crustal arc root. Note the time interval of root foundering shortens when the crustal arc root is involved.

#### 4.4. Mantle-Derived Magma and Arc Root Foundering

Our modeling results suggest that partial melting of the underthrusted crust alone does not generate the volume nor thickening rates needed to produce a magmatic flare-up. Thus, magmatic contributions from other sources are be needed. Crustal melt generated from processes other than partial melting of the underthrusted crust (e.g., burial of fore-arc sediments and relamination) could play a role but their magmatic contribution is not well-quantified. Melt from in situ crustal melting could intensify the magmatism, but such melt does not contribute to the net growth of the arc crust. The other important source of arc magma is from the mantle (e.g., Attia et al., 2020; Bouilhol et al., 2015; Martínez Ardila et al., 2019; Schwartz et al., 2017). For example, a recent zircon Hf isotopes study of the central Sierra Nevada (Attia et al., 2020) and studies on geochemistry and/or Sr, Nd, and Pb isotopes in the North and South Cordilleran arc (Martínez Ardila et al., 2019) and Fiordland arc (Schwartz et al., 2017) all reveal primitive compositions, proposing a mantle source fueled magmatic flare-up events. In the "Cordilleran cycle" model (DeCelles et al., 2009), foundering of the arc root triggers asthenospheric upwelling, resulting in rapid decompression melting (e.g., Kay & Kay, 1993) of the mantle and causing a magmatic pulse that is above the mantle flux baseline (Lee & Anderson, 2015).

In order to highlight the role of mantle melt and how foundering of the arc root regulates the magmatic tempo, we constructed a simple numerical model to illustrate the cycle of lower crustal underthrusting, arc root buildup, foundering, and renewed underthrusting (Figure 10). The model begins assuming that the arc root had just foundered, and the asthenospheric mantle begins to upwell. We use a mantle-derived arc magma generation rate of 1 km/Myr, a 300% increase compared to the baseline (~0.3 km/Myr, 1 AU), to represent the increase of arc magma generation associated with the upwelling; the 300% increase is an arbitrary choice to demonstrate the increased magma produced by adiabatic decompression of the asthenosphere. We let the mantle-derived magma decrease with time mainly due to (1) pinching out of the sub-arc mantle by renewed crustal underthrusting and arc root formation (Chin et al., 2015) and (2) dissipation of upwellings after foundering of the arc root. The arc root in the model is the sum of the root generated via partial melting of the underthrusted crust (e.g., Ducea, 2001, 2002) and the root due to the differentiation of mantle-derived magmas (Lee & Anderson, 2015; Lee et al., 2006; Tang et al., 2019). We refer to the former root as crustal arc root and the latter as the mantle arc root. The model presented here is based on the geometry shown in Figure 2 and has the same initial and boundary conditions as Case 2 of the numerical model:

YANG ET AL. 15 of 19



constant 5 km/Myr underthrusting rate, 2 wt. % water content, and pure conduction with no amplification of thermal diffusivity. The model setup is presented in the supporting information.

Figure 10 shows that with the combined crustal root generated from partial melting of the underthrusted crust and the formation of the mantle root, the critical thickness of root is reached every 36 Myr (green curve in panel c). If there is no underthrusting of the lower crust and formation of the crustal root but only mantle root, the same critical thickness is reached every 69 Myr (dotted purple curve in panel c), roughly twice longer than the former case. Such a difference affects the recurring time of root foundering and potential arc flare-up. It is noted for the simple model presented here, we do not include any additional crustal partial melt and the mechanical process associated with root foundering is ignored. Therefore, the model is incapable of resolving the ratio of crustal versus mantle melts nor the exact timing of root foundering. Chin et al. (2015) and Cao et al. (2016b) suggested that the increasing thickness of the arc upper plate due to magmatic and tectonic thickening also causes a self-limiting effect on arc magmatism and controls the arc magmatism tempo. Here, we use a simple model to highlight that crustal underthrusting plays an important role in limiting arc magma generation and regulating the magmatic tempo via contribution to the arc root formation and foundering.

# 5. Conclusions: Does Underthrusting Crust Feed Arc Magmatic Flare-Up?

Numerical modeling results show that the total volume of arc magma and the magmatic thickening rate associated with partial melting of underthrusting retro-arc lower crust are not sufficient to drive arc flare-up events of similar magnitude as those that occurred in the Cretaceous Sierra Nevada arc. While this study is focused on underthrusting of the retro-arc, the results from our generic model are potentially applicable to the process of fore-arc underthrusting. We demonstrated the total volume of magma generated through partial melting of the underthrusted lower crust depends on the size of the underthrusted lower crustal slab, while the temporal pattern of the magmatic thickening rate is directly correlated with the underthrusting rate and is controlled by the ratio between the characteristic timescales of heat transfer and underthrusting. Crustal underthrusting contributes to the growth of the arc root whose subsequent foundering may regulate the tempo of arc magmatism. We suggest additional melts from the mantle and/or other crustal sources are needed during arc flare-ups.

# **Data Availability Statement**

Data were not used, nor created for this research. Software for this research is not publicly available and software license should be purchased from the MathWorks company (www.mathworks.com).

#### Acknowledgments

This study is supported by the UNR microgrant awarded to Cao and Gordon, National Natural Science Foundation of China (Grant No. 41888101), and National Science Foundation (NSF) grant (EAR-1830139). Ming Tang is thanked for the help with the setup of the MELTS program and Julin Zhang is thanked for the discussion on latent heat. Nicolas Riel and an anonymous reviewer are thanked for their comments. Editor Claudio Faccenna and associate editor Boris Kaus are thanked for handling the manuscript.

# References

- Ardill, K., Paterson, S., & Memeti, V. (2018). Spatiotemporal magmatic focusing in upper-mid crustal plutons of the Sierra Nevada arc. Earth and Planetary Science Letters, 498, 88–100. https://doi.org/10.1016/j.epsl.2018.06.023
- Armstrong, R. L., & Clark, S. P. (1988). Mesozoic and early Cenozoic magmatic evolution of the Canadian Cordillera. *Geological Society of America Special Paper*, 218, 55–91.
- Arndt, N. T., & Goldstein, S. L. (1989). An open boundary between lower continental crust and mantle: Its role in crust formation and crustal recycling. *Tectonophysics*, 161(3-4), 201–212.
- Attia, S., Cottle, J. M., & Paterson, S. R. (2020). Erupted zircon record of continental crust formation during mantle driven arc flare-ups. Geology, 48(5), 446–451. https://doi.org/10.1130/G46991.1
- Bergantz, G. W. (1989). Underplating and partial melting: Implications for melt generation and extraction. *Science*, 245(4922), 1093–1095. Bouilhol, P., Magni, V., van Hunen, J., & Kaislaniemi, L. (2015). A numerical approach to melting in warm subduction zones. *Earth and Planetary Science Letters*, 411, 37–44. https://doi.org/10.1016/j.epsl.2014.11.043
- Cao, W., Kaus, B. J., & Paterson, S. (2016a). Intrusion of granitic magma into the continental crust facilitated by magma pulsing and dike-diapir interactions: Numerical simulations. *Tectonics*, 35(6), 1575–1594. https://doi.org/10.1002/2015TC004076
- Cao, W., Lee, C. T. A., & Lackey, J. S. (2017). Episodic nature of continental arc activity since 750 Ma: A global compilation. Earth and Planetary Science Letters, 461, 85–95. https://doi.org/10.1016/j.epsl.2016.12.044
- Cao, W., & Paterson, S. (2016). A mass balance and isostasy model: Exploring the interplay between magmatism, deformation and surface erosion in continental arcs using central Sierra Nevada as a case study. *Geochemistry, Geophysics, Geosystems*, 17(6), 2194–2212. https://doi.org/10.1002/2015GC006229
- Cao, W., Paterson, S., Saleeby, J., & Zalunardo, S. (2016b). Bulk arc strain, crustal thickening, magma emplacement, and mass balances in the Mesozoic Sierra Nevada arc. *Journal of Structural Geology*, 84, 14–30. https://doi.org/10.1016/j.jsg.2015.11.002

YANG ET AL. 16 of 19



- Cecil, M. R., Rusmore, M. E., Gehrels, G. E., Woodsworth, G. J., Stowell, H. H., Yokelson, I. N., et al. (2018). Along-strike variation in the magmatic tempo of the Coast Mountains batholith, British Columbia, and implications for processes controlling episodicity in arcs. *Geochemistry, Geophysics, Geosystems*, 19(11), 4274–4289. https://doi.org/10.1029/2018GC007874
- Chapman, A. D., Saleeby, J. B., & Eiler, J. (2013). Slab flattening trigger for isotopic disturbance and magmatic flare-up in the southernmost Sierra Nevada batholith, California. *Geology*, 41(9), 1007–1010. https://doi.org/10.1130/G34445.1
- Chapman, J. B., & Ducea, M. N. (2019). The role of arc migration in Cordilleran orogenic cyclicity. *Geology*, 47(7), 627–631. https://doi.org/10.1130/G46117.1
- Chin, E. J., Lee, C. T. A., & Blichert-Toft, J. (2015). Growth of upper plate lithosphere controls tempo of arc magmatism: Constraints from Al-diffusion kinetics and coupled Lu-Hf and Sm-Nd chronology. *Geochemical Perspectives Letters*, 1(1), 20–32. https://doi.org/10.7185/geochemlet.1503
- Chu, X., Lee, C. T. A., Dasgupta, R., & Cao, W. (2019). The contribution to exogenic CO<sub>2</sub> by contact metamorphism at continental arcs: A coupled model of fluid flux and metamorphic decarbonation. *American Journal of Science*, 319(8), 631–657. https://doi.org/10.2475/08.2019.01
- Condie, K. C. (2013). Plate tectonics & crustal evolution. New York, NY: Elsevier.
- Cope, T. (2017). Phanerozoic magmatic tempos of North China. Earth and Planetary Science Letters, 468, 1–10. https://doi.org/10.1016/j.epsl.2017.03.022
- DeCelles, P. G. (2004). Late Jurassic to Eocene evolution of the Cordilleran thrust belt and foreland basin system, western USA. *American Journal of Science*, 304(2), 105–168. https://doi.org/10.2475/ajs.304.2.105
- DeCelles, P. G., Ducea, M. N., Kapp, P., & Zandt, G. (2009). Cyclicity in Cordilleran orogenic systems. *Nature Geoscience*, 2(4), 251. https://doi.org/10.1038/ngeo469
- DeCelles, P. G., & Graham, S. A. (2015). Cyclical processes in the North American Cordilleran orogenic system. *Geology*, 43(6), 499–502. https://doi.org/10.1130/G36482.1
- Decelles, P. G., Zandt, G., Beck, S. L., Currie, C. A., Ducea, M. N., Kapp, P., et al. (2014). Cyclical orogenic processes in the Cenozoic central Andes. *Geological Society of America Memoirs*, 212, MWR212–22. https://doi.org/10.1130/2015.1212(22)
- De Silva, S. L., Riggs, N. R., & Barth, A. P. (2015). Quickening the pulse: Fractal tempos in continental arc magmatism. *Elements*, 11(2), 113–118. https://doi.org/10.2113/gselements.11.2.113
- Ducea, M. N. (2001). The California arc: Thick granitic batholiths, eclogitic residues, lithospheric-scale thrusting, and magmatic flare-ups. *GSA Today*, 11(11), 4–10. https://doi.org/10.1130/1052-5173(2001)011%3C0004:TCATGB%3E2.0.CO;2
- Ducea, M. N. (2002). Constraints on the bulk composition and root foundering rates of continental arcs: A California arc perspective. Journal of Geophysical Research, 107(B11), ECV-15. https://doi.org/10.1029/2001JB000643
- Ducea, M. N., & Barton, M. D. (2007). Igniting flare-up events in Cordilleran arcs. *Geology*, 35(11), 1047–1050. https://doi.org/10.1130/
- Ducea, M. N., & Chapman, A. D. (2018). Sub-magmatic arc underplating by trench and forearc materials in shallow subduction systems; A geologic perspective and implications. *Earth-Science Reviews*, 185, 763–779. https://doi.org/10.1016/j.earscirev.2018.08.001
- Ducea, M. N., Chapman, A. D., Bowman, E., & Triantafyllou, A. (2020). Arclogites and their role in continental evolution; part 1: Background, locations, petrography, geochemistry, chronology and thermobarometry. *Earth-Science Reviews*, 103375. http://dx.doi.org/10.1016/j.earscirev.2020.103375
- Ducea, M. N., & Saleeby, J. B. (1996). Buoyancy sources for a large, unrooted mountain range, the Sierra Nevada, California: Evidence from xenolith thermobarometry. *Journal of Geophysical Research*. 101(B4), 8229–8244.
- England, P., Molnar, P., & Richter, F. (2007). John Perry's neglected critique of Kelvin's age for the Earth: A missed opportunity in geodynamics. GSA Today, 17(1), 4–9. https://doi.org/10.1130/GSAT01701A.1
- Erdman, M. E., & Lee, C. T. A. (2014). Oceanic-and continental-type metamorphic terranes: Occurrence and exhumation mechanisms. *Earth-Science Reviews*, 139, 33–46. https://doi.org/10.1016/j.earscirev.2014.08.012
- Gehrels, G., Rusmore, M., Woodsworth, G., Crawford, M., Andronicos, C., Hollister, L., et al. (2009). U-Th-Pb geochronology of the Coast Mountains batholith in north-coastal British Columbia: Constraints on age and tectonic evolution. *Geological Society of America Bulle-tin*, 121(9–10), 1341–1361. https://doi.org/10.1130/B26404.1
- Ghiorso, M. S., & Sack, R. O. (1995). Chemical mass transfer in magmatic processes IV. A revised and internally consistent thermodynamic model for the interpolation and extrapolation of liquid-solid equilibria in magmatic systems at elevated temperatures and pressures. *Contributions to Mineralogy and Petrology*, 119(2–3), 197–212.
- Hacker, B. R., Kelemen, P. B., & Behn, M. D. (2011). Differentiation of the continental crust by relamination. *Earth and Planetary Science Letters*, 307(3–4), 501–516. https://doi.org/10.1016/j.epsl.2011.05.024
- Hajná, J., Žák, J., & Dörr, W. (2017). Time scales and mechanisms of growth of active margins of Gondwana: A model based on detrital zircon ages from the Neoproterozoic to Cambrian Blovice accretionary complex, Bohemian Massif. *Gondwana Research*, 42, 63–83. https://doi.org/10.1016/j.gr.2016.10.004
- Haschke, M., Günther, A., Melnick, D., Echtler, H., Reutter, K. J., Scheuber, E., & Oncken, O. (2006). Central and southern Andean tectonic evolution inferred from arc magmatism. In O. Oncken, G. Chong, G. Franz, P. Giese, H. Götze, V. Ramos, M. Strecker & P. Wigger (Eds.), *The Andes* (pp. 337–353). Berlin, Heidelberg: Springer. https://doi.org/10.1007/978-3-540-48684-8\_16
- Jaupart, C., & Mareschal, J. C. (2010). Heat generation and transport in the Earth. Cambridge, MA: Cambridge University Press.
- Jiang, H., & Lee, C. T. A. (2017). Coupled magmatism–erosion in continental arcs: Reconstructing the history of the Cretaceous Peninsular Ranges batholith, southern California through detrital hornblende barometry in forearc sediments. *Earth and Planetary Science Letters*, 472, 69–81. https://doi.org/10.1016/j.epsl.2017.05.009
- Jicha, B. R., & Jagoutz, O. (2015). Magma production rates for intraoceanic arcs. *Elements*, 11(2), 105–111. https://doi.org/10.2113/gselements.11.2.105
- Karakas, O., & Dufek, J. (2015). Melt evolution and residence in extending crust: Thermal modeling of the crust and crustal magmas. Earth and Planetary Science Letters, 425, 131–144. https://doi.org/10.1016/j.epsl.2015.06.001
- Karlstrom, L., Lee, C. T., & Manga, M. (2014). The role of magmatically driven lithospheric thickening on arc front migration. *Geochemistry, Geophysics, Geosystems*, 15(6), 2655–2675. https://doi.org/10.1002/2014GC005355
- Kay, R. W., & Kay, S. M. (1993). Delamination and delamination magmatism. *Tectonophysics*, 219(1-3), 177-189.
- Keller, T., May, D. A., & Kaus, B. J. (2013). Numerical modelling of magma dynamics coupled to tectonic deformation of lithosphere and crust. *Geophysical Journal International*, 195(3), 1406–1442. https://doi.org/10.1093/gji/ggt306
- Kirsch, M., Paterson, S. R., Wobbe, F., Ardila, A. M. M., Clausen, B. L., & Alasino, P. H. (2016). Temporal histories of Cordilleran continental arcs: Testing models for magmatic episodicity. *American Mineralogist*, 101(10), 2133–2154. https://doi.org/10.2138/am-2016-5718

YANG ET AL. 17 of 19



- Lange, R. A., Cashman, K. V., & Navrotsky, A. (1994). Direct measurements of latent heat during crystallization and melting of a ugandite and an olivine basalt. Contributions to Mineralogy and Petrology, 118(2), 169–181.
- Lee, C. T. A. (2014). The physics and chemistry of recycling lower continental crust. *Treatise of Geochemistry*, 4, 423–456. https://doi.org/10.1016/B978-0-08-095975-7.00314-4
- Lee, C. T. A., & Anderson, D. L. (2015). Continental crust formation at arcs, the arclogite "delamination" cycle, and one origin for fertile melting anomalies in the mantle. Science Bulletin, 60(13), 1141–1156. https://doi.org/10.1007/s11434-015-0828-6
- Lee, C. T. A., Cheng, X., & Horodyskyj, U. (2006). The development and refinement of continental arcs by primary basaltic magmatism, garnet pyroxenite accumulation, basaltic recharge and delamination: Insights from the Sierra Nevada, California. Contributions to Mineralogy and Petrology, 151(2), 222–242. https://doi.org/10.1007/s00410-005-0056-1
- Lee, C. T. A., Thurner, S., Paterson, S., & Cao, W. (2015a). The rise and fall of continental arcs: Interplays between magmatism, uplift, weathering, and climate. *Earth and Planetary Science Letters*, 425, 105–119. https://doi.org/10.1016/j.epsl.2015.05.045
- Lee, C. T. A., Morton, D. M., Farner, M. J., & Moitra, P. (2015b). Field and model constraints on silicic melt segregation by compaction/hindered settling: The role of water and its effect on latent heat release. *American Mineralogist*, 100(8–9), 1762–1777. https://doi.org/10.2138/am-2015-5121
- Li, X. H., Li, Z. X., Li, W. X., Liu, Y., Yuan, C., Wei, G., & Qi, C. (2007). U-Pb zircon, geochemical and Sr-Nd-Hf isotopic constraints on age and origin of Jurassic I-and A-type granites from central Guangdong, SE China: A major igneous event in response to foundering of a subducted flat-slab? *Lithos*, 96(1-2), 186-204. https://doi.org/10.1016/j.lithos.2006.09.018
- Liang, Y., & Parmentier, E. M. (2010). A two-porosity double lithology model for partial melting, melt transport and melt–rock reaction in the mantle: Mass conservation equations and trace element transport. *Journal of Petrology*, 51(1–2), 125–152. https://doi.org/10.1093/petrology/egp086
- Mallik, A., & Dasgupta, R. (2012). Reaction between MORB-eclogite derived melts and fertile peridotite and generation of ocean island basalts. *Earth and Planetary Science Letters*, 329, 97–108. https://doi.org/10.1016/j.epsl.2012.02.007
- Martínez Ardila, A. M., Paterson, S. R., Memeti, V., Parada, M. A., & Molina, P. G. (2019). Mantle driven cretaceous flare-ups in Cordilleran arcs. Lithos, 326, 19–27. https://doi.org/10.1016/j.lithos.2018.12.007
- McKenzie, N. R. (2017). Zircons reveal ancient perturbations. *Nature Geoscience*, 10(12), 884–886. https://doi.org/10.1038/s41561-017-0023-2 Moghadam, H. S., Li, X. H., Griffin, W. L., Stern, R. J., Thomsen, T. B., Meinhold, G., et al. (2017). Early Paleozoic tectonic reconstruction of Iran: Tales from detrital zircon geochronology. *Lithos*, 268, 87–101. https://doi.org/10.1016/j.lithos.2016.09.008
- Mottaghy, D., Vosteen, H. D., & Schellschmidt, R. (2008). Temperature dependence of the relationship of thermal diffusivity versus thermal conductivity for crystalline rocks. *International Journal of Earth Sciences*, 97(2), 435–442. https://doi.org/10.1007/s00531-007-0238-3
- Paterson, S. R., & Ducea, M. N. (2015). Arc magmatic tempos: Gathering the evidence. *Elements*, 11(2), 91–98. https://doi.org/10.2113/gselements.11.2.91
- Paulsen, T., Deering, C., Sliwinski, J., Bachmann, O., & Guillong, M. (2016). A continental arc tempo discovered in the Pacific-Gondwana margin mudpile? *Geology*, 44(11), 915–918. https://doi.org/10.1130/G38189.1
- Pearson, D. M., MacLeod, D. R., Ducea, M. N., Gehrels, G. E., & Jonathan Patchett, P. (2017). Sediment underthrusting within a continental magmatic arc: Coast Mountains batholith, British Columbia. *Tectonics*, 36(10), 2022–2043. https://doi.org/10.1002/2017TC004594
- Pepper, M., Gehrels, G., Pullen, A., Ibanez-Mejia, M., Ward, K. M., & Kapp, P. (2016). Magmatic history and crustal genesis of western South America: Constraints from U-Pb ages and Hf isotopes of detrital zircons in modern rivers. *Geosphere*, 12(5), 1532–1555. https://doi.org/10.1130/GES01315.1
- Pilger, R. H. (1984). Cenozoic plate kinematics, subduction and magmatism: South American Andes. *Journal of the Geological Society*, 141(5), 793–802.
- Ratschbacher, B. C., Paterson, S. R., & Fischer, T. P. (2019). Spatial and depth-dependent variations in magma volume addition and addition rates to continental arcs: Application to global CO<sub>2</sub> fluxes since 750 Ma. *Geochemistry, Geophysics, Geosystems*, 20(6), 2997–3018. https://doi.org/10.1029/2018GC008031
- Rees Jones, D. W., Katz, R. F., Tian, M., & Rudge, J. F. (2018). Thermal impact of magmatism in subduction zones. *Earth and Planetary Science Letters*, 481, 73–79. https://doi.org/10.1016/j.epsl.2017.10.015
- Reymer, A., & Schubert, G. (1984). Phanerozoic addition rates to the continental crust and crustal growth. Tectonics, 3(1), 63-77.
- Rosenberg, C. L., & Handy, M. R. (2005). Experimental deformation of partially melted granite revisited: Implications for the continental crust. *Journal of Metamorphic Geology*, 23(1), 19–28. https://doi.org/10.1111/j.1525-1314.2005.00555.x
- Rudnick, R. L. (1995). Making continental crust. *Nature*, 378(6557), 571-578.
- Rudnick, R. L., & Gao, S. (2003). Composition of the continental crust. *The Crust*, *3*, 1–64. https://doi.org/10.1016/B0-08-043751-6/03016-4 Rummel, L., Kaus, B. J., Baumann, T. S., White, R. W., & Riel, N. (2020). Insights into the Compositional Evolution of Crustal Magmatic Systems from Coupled Petrological-Geodynamical Models. *Journal of Petrology*, *61*, (2), 1–36. http://dx.doi.org/10.1093/petrology/egaa029
- Sauer, K. B., Gordon, S. M., Miller, R. B., Vervoort, J. D., & Fisher, C. M. (2017). Transfer of metasupracrustal rocks to midcrustal depths in the North Cascades continental magmatic arc, Skagit Gneiss Complex, Washington. *Tectonics*, 36(12), 3254–3276. https://doi.org/10.1002/2017TC004728
- Sauer, K. B., Gordon, S. M., Miller, R. B., Vervoort, J. D., & Fisher, C. M. (2018). Provenance and metamorphism of the Swakane Gneiss: Implications for incorporation of sediment into the deep levels of the North Cascades continental magmatic arc, Washington. *Lithosphere*, 10(3), 460–477. https://doi.org/10.1016/j.earscirev.2018.08.001
- Sawyer, E. W. (1994). Melt segregation in the continental crust. Geology, 22(11), 1019-1022.
- Schwartz, J. J., Klepeis, K. A., Sadorski, J. F., Stowell, H. H., Tulloch, A. J., & Coble, M. A. (2017). The tempo of continental arc construction in the Mesozoic Median Batholith, Fiordland, New Zealand. *Lithosphere*, 9(3), 343–365. https://doi.org/10.1130/L610.1
- Stern, R. J. (2002). Subduction zones. Reviews of Geophysics, 40(4), 3-1. http://dx.doi.org/10.1029/2001rg000108
- Syracuse, E. M., van Keken, P. E., & Abers, G. A. (2010). The global range of subduction zone thermal models. *Physics of the Earth and Planetary Interiors*, 183(1–2), 73–90. https://doi.org/10.1016/j.pepi.2010.02.004
- Tang, M., Lee, C. T. A., Chen, K., Erdman, M., Costin, G., & Jiang, H. (2019). Nb/Ta systematics in arc magma differentiation and the role of arclogites in continent formation. *Nature Communications*, 10(1), 1–8. https://doi.org/10.1038/s41467-018-08198-3
- Tsujimori, T., Sisson, V. B., Liou, J. G., Harlow, G. E., & Sorensen, S. S. (2006). Very-low-temperature record of the subduction process: A review of worldwide lawsonite eclogites. *Lithos*, 92(3–4), 609–624. https://doi.org/10.1016/j.lithos.2006.03.054
- review of worldwide lawsonite eclogites. *Lithos*, 92(3–4), 609–624. https://doi.org/10.1016/j.lithos.2006.03.054

  Vosteen, H. D., & Schellschmidt, R. (2003). Influence of temperature on thermal conductivity, thermal capacity and thermal diffusivity for dif-
- ferent types of rock. *Physics and Chemistry of the Earth, Parts A/B/C, 28*(9–11), 499–509. https://doi.org/10.1016/S1474-7065(03)00069-X Whittington, A. G., Hofmeister, A. M., & Nabelek, P. I. (2009). Temperature-dependent thermal diffusivity of the Earth's crust and implications for magmatism. *Nature*, 458(7236), 319–321. https://doi.org/10.1038/nature07818

YANG ET AL. 18 of 19





- Yonkee, W. A., & Weil, A. B. (2015). Tectonic evolution of the Sevier and Laramide belts within the North American Cordillera orogenic system. *Earth-Science Reviews*, 150, 531–593. https://doi.org/10.1016/j.earscirev.2015.08.001
- Yu, X., & Lee, C. T. A. (2016). Critical porosity of melt segregation during crustal melting: Constraints from zonation of peritectic garnets in a dacite volcano. *Earth and Planetary Science Letters*, 449, 127–134. https://doi.org/10.1016/j.epsl.2016.05.025
- Zhang, X., Chung, S. L., Lai, Y. M., Ghani, A. A., Murtadha, S., Lee, H. Y., & Hsu, C. C. (2019). A 6000-km-long Neo-Tethyan arc system with coherent magmatic flare-ups and lulls in South Asia. *Geology*, 47(6), 573–576. https://doi.org/10.1130/G46172.1
- Zhang, Z., Zhao, G., Santosh, M., Wang, J., Dong, X., & Shen, K. (2010). Late Cretaceous charnockite with adaktic affinities from the Gangdese batholith, southeastern Tibet: Evidence for Neo-Tethyan mid-ocean ridge subduction? *Gondwana Research*, 17(4), 615–631. https://doi.org/10.1016/j.gr.2009.10.007
- Zhu, D. C., Wang, Q., Zhao, Z. D., Chung, S. L., Cawood, P. A., Niu, Y., et al. (2015). Magmatic record of India-Asia collision. *Scientific Reports*, 5, 14289. https://doi.org/10.1038/srep14289

YANG ET AL. 19 of 19